Earth and Planetary Science Letters 584 (2022) 117503

Contents lists available at ScienceDirect

Earth and Planetary Science Letters

www.elsevier.com/locate/epsl

Binding and transport of Cr(III) by clay minerals during the Great Oxidation Event

Weiduo Hao [a,*], Ning Chen [b], Wenyuan Sun [c], Kaarel Mänd [a,d], Kalle Kirsimäe [d], Yoram Teitler [e], Peeter Somelar [d], Leslie J. Robbins [f], Michael G. Babechuk [g], Noah J. Planavsky [h], Daniel S. Alessi [a], Kurt O. Konhauser [a]

[a] Department of Earth & Atmospheric Sciences, University of Alberta, Edmonton, Alberta, T6G 2E3, Canada
[b] Canadian Light Source Inc., University of Saskatchewan, Saskatoon, Saskatchewan, S7N 0X4, Canada
[c] Department of Mechanical Engineering, University of Alberta, Edmonton, Alberta, T6G 2H5, Canada
[d] Department of Geology, University of Tartu, Tartu 50411, Estonia
[e] Université de Lorraine-CNRS, GeoRessources laboratory, 54500 Nancy, France
[f] Department of Geology, University of Regina, Regina, Saskatchewan, S4S 0A2, Canada
[g] Department of Earth Sciences, Memorial University, St. John's, Newfoundland & Labrador, A1B 3X5, Canada
[h] Department of Earth and Planetary Sciences, Yale University, New Haven, CT 06511, USA

ARTICLE INFO

Article history:
Received 21 August 2021
Received in revised form 11 March 2022
Accepted 13 March 2022
Available online xxxx
Editor: B. Wing

Keywords:
Cr(III)
iron formation
clay transportation
EXAFS

ABSTRACT

A spike in chromium (Cr) abundance above crustal background in iron formations post-dating the Great Oxidation Event (ca. 2.5-2.3 billion years ago) has been suggested to reflect the evolution of terrestrial aerobic pyrite and siderite oxidation and the initiation of widespread acid rock drainage that would enhance Cr transport from terrestrial weathering environments to the oceans. However, it remains unclear whether Cr was transported in a soluble form (as Cr(III) or Cr(VI)), or bound to particulate surfaces. Here, we experimentally investigate the binding mechanisms of Cr(III) – the typical oxidation state associated with primary igneous minerals such as chromite – to three common soil clay minerals (kaolinite, illite, and montmorillonite) using extended X-ray adsorption fine structure (EXAFS) spectroscopy. Our results demonstrate that Cr(III) precipitates on the clay surfaces over a pH range of 6 to 8 as guyanaite (β-CrOOH) due to the replacement of surface Al-octahedra by paired Cr(III) octahedra. Bidentate bonding with a Cr-Cr interatomic distance of 3.43-3.51 Å indicates the incorporation of Cr(III) into the clay structure. A comparison between Cr(III) adsorption/precipitation onto the three clays and the desorption of Cr(III) from Cr(III)-spiked clays shows that kaolinite has the highest retention capacity for Cr(III), a predictable result given that an entire Al-octahedral sheet is exposed for Cr(III) binding, while illite and montmorillonite only have Al-edge sites. Moreover, Cr(III) was essentially immobilized in our experiments except under very acidic conditions (pH<2). Extending our results to the interpretation of the Cr record in iron formations, we suggest that under intense chemical weathering conditions, not only did acidity promote the solubilization of Cr(III) from primary Cr-bearing minerals, but that parent rocks were more systematically weathered to an advanced state dominated by kaolinite – creating ideal conditions for Cr adsorption. Erosion of regolith that scavenged mobilized Cr(III) could then facilitate transport of Cr(III)-bearing kaolinite to coastal environments where it contributed to the super-crustal Cr abundances above detrital background preserved in ca. 2.5-2.0 Ga iron formations.

1. Introduction

The geochemical cycling of chromium (Cr), its isotopic fractionation, and incorporation into various sedimentary rocks have been studied to help shape the narrative of Earth's oceanic and atmospheric oxidation state through time (e.g., Frei et al., 2009; Konhauser et al., 2011; Crowe et al., 2013; Reinhard et al., 2013; Planavsky et al., 2014; Gilleaudeau et al., 2016; Albut et al., 2018; Canfield et al., 2018; Toma et al., 2019). Utilizing the Cr record as a redox proxy relies on understanding the factors that control the mobility, and ultimately fate, of Cr beginning with chemical weathering of source rocks on land, through physical or chemical transport to the oceans, deposition in sediment, and any re-

* Corresponding author at: 3-11 Earth Sciences Building, University of Alberta, Edmonton, AB, T6G 2E3, Canada.
E-mail address: whao@ualberta.ca (W. Hao).

https://doi.org/10.1016/j.epsl.2022.117503
0012-821X/

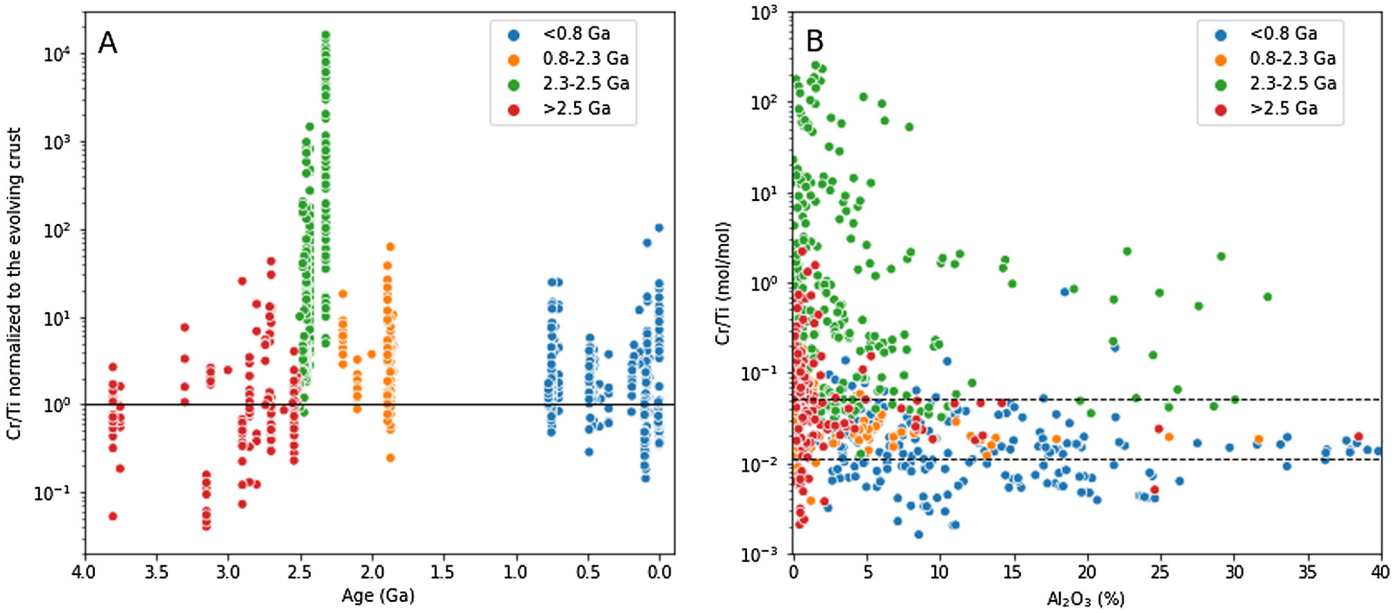

Fig. 1. The database for Cr/Ti ratios in IF. (A) Normalized Cr/Ti ratios in IF as a function of geological time; (B) Cross-plot of Al_2O_3 abundance versus molar Cr/Ti ratios in IF samples. The upper and lower dashed lines in panel B correspond to the molar Cr/Ti ratios expected for upper continental crust from 3.5 to 2.5 Ga and <0.2 Ga, respectively, based on the restoration model of Condie (1993). Updated from Konhauser et al. (2011). (For interpretation of the colors in the figures, the reader is referred to the web version of this article.)

dox transformations along the way. In brief, today the majority of dissolved seawater Cr is sourced from riverine inputs, as Cr(VI) formed by the oxidative weathering of chromite [$(Fe,Mg)Cr(III)_2O_4$] or Cr(II/III)-bearing silicate minerals such as olivine and pyroxene (Fendorf and Zasoski, 1992). The only important, naturally occurring oxidants of dissolved Cr(III) at pH<9 are Mn(III)- and Mn(IV)-oxides (e.g., birnessite, MnO_2) (Eary and Rai, 1987; Oze et al., 2007). Aqueous Cr(III) has a very low solubility under most surficial aqueous Eh-pH conditions. Specifically, it is readily re-precipitated as $(Fe,Cr)(OH)_3$ close to the source at pH values greater than 6.3. However, at pH <6.3, $Cr(OH)^{2+}$ dominates at low Eh, and at pH <4 Cr^{3+} becomes the dominant aqueous species, even under high Eh conditions (Rai et al., 1989). Some organic and inorganic Cr(III)-complexes also likely have an uncommon but important role in aiding its solubility in some hydrothermal and terrestrial environments (McClain and Maher, 2016; Saad et al., 2017).

Based on elevated Cr/Ti ratios preserved in some shallow-water iron formations (IFs) deposited between 2.45 to 2.32 billion years ago (Fig. 1A), and the lack of major Cr isotopic fractionation in this time period that would be indicative of oxidative weathering that produces the soluble Cr(VI) oxyanion, Konhauser et al. (2011) hypothesized that high chemical weathering rates combined with low pH conditions were required to solubilize Cr from mafic rocks and soils. The confluence of both factors was linked to acidity generated through the bacterial oxidation of a crustal pyrite reservoir that coincided with the initial rise of oxygen in the atmosphere – the Great Oxidation Event (GOE). Those authors suggested that dissolved Cr^{3+} or $Cr(OH)^{2+}$ was then transported to the oceans via acidic streams or groundwater, and upon mixing with seawater, would have rapidly precipitated out of solution as a $(Fe,Cr)(OH)_3$ phase. However, rivers and groundwater with low pH would be naturally buffered by higher alkalinity waters flowing through non-acid-generating rock types (i.e., silicate weathering reactions that control the carbonic acid system). Therefore, much of the Cr(III) mobilized by this pulse of low-pH oxidative weathering presumably never made it to the oceans, instead being lost from solution along catchment pathways. Accordingly, we suggest that the elevated Cr found in the 2.45 to 2.32 Ga IF may be related, in large part, to an alternative mode of Cr transport, namely the erosion and subsequent transport of suspended sediments with anomalous Cr enrichments.

In modern weathering profiles, the most significant sink for Cr(III) is its association with Fe(III) (oxyhydr)oxides, such as ferrihydrite [$Fe(OH)_3$], goethite [FeO(OH)], and hematite (Fe_2O_3). Indeed, the close association of Cr with Fe(III) (oxyhydr)oxides is most clearly manifested in the Fe- and Al-rich weathering profiles – laterites and bauxites – that commonly form in tropical environments that experience high rates of chemical weathering (Widdowson, 2007). The geochemical mechanisms underpinning the accumulation of Cr in laterites are reasonably well understood. The process generally involves Cr(III) either adsorbing to existing Fe(III) (oxyhydr)oxides (Oze et al., 2004), potentially followed by substitution of Cr(III) into the (oxyhydr)oxide structure (Trolard et al., 1995), or its co-precipitation with dissolved Fe(III) to form phases such as $(Cr,Fe)(OH)_3$ (Rai et al., 1989). However, at low pH conditions, Fe(III) (oxyhydr)oxide solubility increases dramatically and Fe^{3+} becomes the dominant oxidant for pyrite in acid drainage environments (Singer and Stumm, 1970) like that envisioned by Konhauser et al. (2011) immediately following the onset of the GOE. Immediately following the initiation of the GOE (assuming O_2 accumulation beginning ca. 2.45 Ga), however, there is no evidence that weathering profiles accumulated appreciable Fe(III) (oxyhydr)oxides (i.e., there is no evidence for Fe retention in paleosols or red beds preserved until ca. 2.3 Ga; see Farquhar et al., 2011 and Rye and Holland, 1998): even in the ~2.24 Ga Hekpoort paleosols there is still iron loss at depth in the profiles (Yang and Holland, 2003). Depending on the parent rock type, it is possible that residual sulfide and silicate mineral phases (e.g., chlorite, serpentine group minerals) may account for some of the Cr enrichments in weathering profiles (Zeissink, 1969; Berger and Frei, 2014). Other studies, however, have drawn attention to the role of the thermodynamically stable clay minerals formed during weathering – including smectites such as montmorillonite [$(Na,Ca)_{0.33}(Al,Mg)_2(Si_4O_{10})(OH)_2 \cdot nH_2O$], illite [$(Al_2)(Si_{4-x}Al_x)O_{10}(OH)_2 \cdot K_{1-x}$]), and kaolinite [$Al_2Si_2O_5(OH)_4$] – in the retention of Cr in weathering profiles (Boski and Herbosch, 1990).

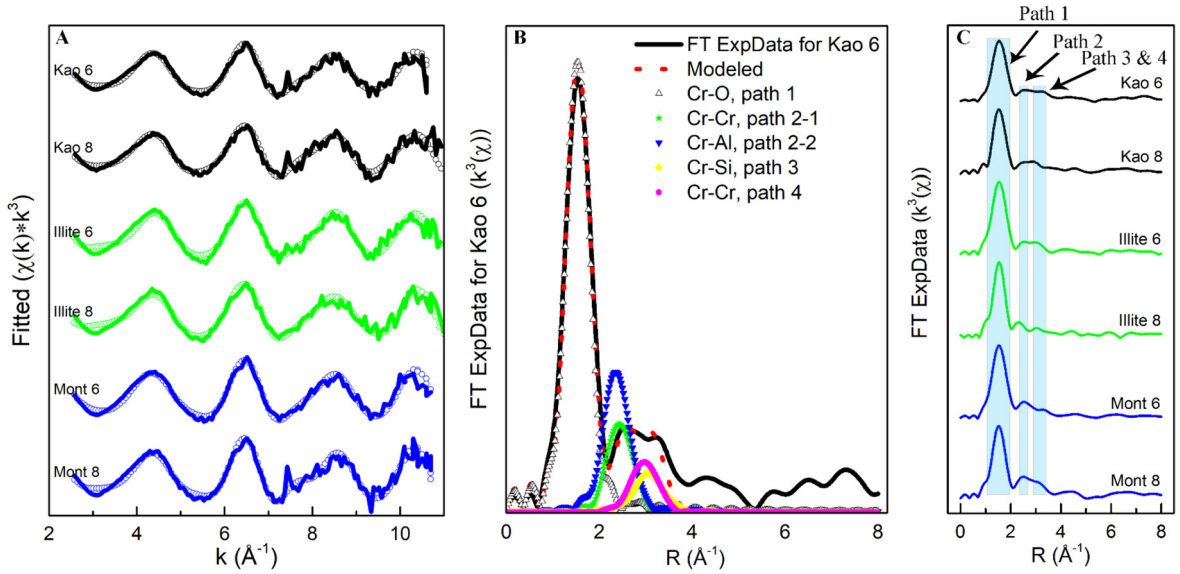

Fig. 2. EXAFS spectra of Cr(III) precipitated onto kaolinite, illite and montmorillonite. (A) EXAFS spectra are k^3 weighted; lines are experimental data; and the circles are model fits to the data. (B) comparison in the magnitude of Fourier transform (FT) among experimental data (black solid line), Feff guided R space curve fitting (red dash line), and FT for the specific paths involved in the R space fitting (using Kao 6 as an example). (C) magnitudes of Fourier transformed EXAFS functions (R-space) with specific paths labeled.

Clay minerals are highly enriched in weathering profiles, and due to high surface areas and an inherent negative surface charge, they typically have a high affinity for the adsorption of trace elements such as Cr(III) (Sarı et al., 2007; Hao et al., 2019). For example, Ni-bearing Fe-rich smectite (nontronite), Fe-montmorillonite, and kaolinite developed on an ultramafic parent rock, can incorporate up to 0.9, 1.9, and 1.6 wt.% of Cr_2O_3, respectively (Kadir et al., 2015). Despite the known affinity of Cr(III) to clay minerals (Griffin et al., 1977; Sajidu et al., 2008), to the best of our knowledge, there is a paucity of research on the molecular-scale mechanisms of Cr(III) uptake by those clay minerals. This is a significant shortcoming – a better understanding of Cr mobility and accumulation in weathering profiles is dependent upon improving the accuracy of models for Cr(III) adsorption and precipitation.

Here, we investigated the coordination environment of Cr(III) on three common clay minerals – kaolinite, illite, and montmorillonite – using synchrotron-based X-ray adsorption spectroscopy (XAS). The three clays were selected to reflect a progressive weathering sequence: from less weathered (illite) to intermediate (montmorillonite) and highly weathered (kaolinite). Our primary objective was to describe how Cr(III) bonds to clay mineral surfaces and to evaluate the stability of such bonds. We then use this new understanding to consider the implications for the geochemical cycling of Cr(III), namely a possibly underappreciated mechanism of transport to the oceans and accumulation in chemical sedimentary rocks such as iron formations.

2. Methods

Briefly, kaolinite (KGa-2), montmorillonite (SWy-2), and illite (IMt-2) were purchased from the Clay Mineral Society, and the clay samples were saturated with Na^+ and size fractionated to remove impurities. To investigate the manner of Cr(III) precipitation onto clay mineral surfaces, Cr(III) precipitation experiments were performed for each of the three clays at pH 6 and 8. The Cr(III)-spiked clays were then transported to the Canadian Light Source in Saskatoon, Canada, for extended X-ray fine structure analysis (EXAFS). Obtained spectra were processed and analyzed using ATHENA in the DEMETER software package, and WinXAS (version 2.3), respectively. Chromium adsorption structural models were generated using Avogadro 1.2, and the proposed models were applied in X-ray absorption near edge structure (XANES) calculations using the FDMNES code. Detailed methods are provided in the *Supplementary Material*. Comparisons between Cr(III) adsorption/precipitation onto the three clays and the desorption of Cr(III) from Cr(III)-spiked clay under different pH conditions were performed to determine the Cr retention capacity of the three clay minerals (see *Supplementary Material*).

Chromium, Ti, and Al concentrations in IF were updated from Konhauser et al. (2011). Briefly, we combined original analyses with a comprehensive literature survey to build a database of representative IF analyses through time, with an emphasis on the Fe-oxide-rich layers. The sample set encompassed a range of IF samples including Algoma- and Superior-type IFs, granular IFs, ironstones, and Phanerozoic hydrothermal deposits (see Konhauser et al., 2011 for details).

3. Results and discussion

3.1. Local structure of Cr(III) precipitates on clay mineral surfaces

Fig. 2A shows Cr EXAFS K-edge $k^3\chi(k)$ spectra for the precipitation of Cr(III) on the surfaces of kaolinite, illite, and montmorillonite, while R space fits of the imaginary part and magnitude are shown in Fig. S1. A Cr-O octahedral structure successfully fits the first shell with a coordination number of approximately 6 and an interatomic distance of 1.98-1.99 Å (path 1 in Table 1, Fig. 2B&C); this structure has been previously observed for Cr(III) precipitates formed on silica, ferric (oxyhydr)oxides, and various organic compounds (Table S1, see references in *Supplementary Material*). Interestingly, differences in the Cr(III) first-shell coordination between the pH 6 and pH 8 systems are not observed, indicating that solution pH has limited impact on the Cr-O octahedral structure in the tested range.

The second shell is composed of a Cr-Al path and a Cr-Cr path, indicating the formation of Cr precipitates (Cr-Cr) on the Al site (Cr-Al) of clay minerals. The Cr-Cr path (path 2-2 in Table 1, Fig. 2B&C) at 2.79-2.97 Å, with a coordination number of approximately 1, corresponds to a bidentate mononuclear complex (edge sharing between Cr-octahedra). Such edge sharing of Cr octahedra has been observed in Cr(III) precipitates (Table S1, see references

Table 1
Structural information derived from EXAFS fitting of Cr(III) adsorption onto clay minerals.

Path#	Path	Kao-8				Kao-6			
		CN	R	DW	E0 /residual	CN	R	DW	E0 /residual
1	Cr-O	5.7	1.99	0.0019	1.0 5.6	5.7	1.99	0.0019	2.0 7.4
2-1	Cr-Al	2.4	2.85	0.0021		2.4	2.84	0.0019	
2-2	Cr-Cr	1.0	2.87	0.0025		0.9	2.86	0.0020	
3	Cr-Si	1.8	3.59	0.0080		2.4	3.65	0.0075	
4	Cr-Cr	1.4	3.44	0.0045		1.3	3.45	0.0058	
Path#	Path	Mont-8				Mont-6			
		CN	R	DW	E0 /residual	CN	R	DW	E0 /residual
1	Cr-O	6.2	1.98	0.0016	0.5 7.0	6.3	1.99	0.0016	1.9 8.8
2-1	Cr-Al	1.8	2.81	0.0021		1.8	2.81	0.0040	
2-2	Cr-Cr	0.7	2.97	0.0021		0.7	2.96	0.0050	
3	Cr-Si	4.8	3.60	0.0074		2.0	3.65	0.0074	
4	Cr-Cr	1.2	3.49	0.0045		1.1	3.45	0.0052	
Path#	Path	Illite-8				Illite-6			
		CN	R	DW	E0 /residual	CN	R	DW	E0 /residual
1	Cr-O	6.0	1.98	0.0016	−1.9 8.1	6.0	1.99	0.0016	1.5 9.9
2-1	Cr-Al	3.8	2.82	0.0021		3.8	2.80	0.0023	
2-2	Cr-Cr	1.3	2.83	0.0021		1.3	2.79	0.0021	
3	Cr-Si	4.4	3.56	0.0074		4.4	3.63	0.0100[a]	
4	Cr-Cr	1.2	3.51	0.0045		1.2	3.43	0.0075	

Note: "a" is upper limit of parameter floating of DW factor; Kao-8 is the Cr(III) adsorption onto kaolinite at pH 8, while Kao-6 is the Cr(III) adsorption onto kaolinite at pH 6. Mont-8 is the Cr(III) adsorption onto montmorillonite at pH 8, while Mont-6 is the Cr(III) adsorption onto montmorillonite at pH 6; Illite-8 is the Cr(III) adsorption onto illite at pH 8, while Illite-6 is the Cr(III) adsorption onto illite at pH 6.

in *Supplementary Material*) and represents a typical structure for bonding individual Cr-octahedra within a larger structure consisting of chained Cr-octahedra (Ichikawa et al., 1999). The Cr-Al path (path 2-1 in Table 1, Fig. 2B&C), with an interatomic distance of 2.81-2.85 Å for all the three clay minerals, indicates Cr-octahedra edge-sharing with Al-octahedra on the surfaces of clay minerals. Sajidu et al. (2008) studied Cr(III) adsorption onto natural clay minerals and found Cr(III) is adsorbed in the form of a chain structure, but the adsorption site was not specified. The existence of edge sharing between Cr-octahedra and Al-octahedra revealed by our EXAFS fitting confirms that Cr(III) forms surface precipitates with Al-OH groups on the clay mineral surfaces. However, it is possible that a minor outer-sphere Cr(III) complex exists, but is undetectable by EXAFS.

Previous studies found that Cr(III) precipitates formed on silica and hydrous ferric oxides have a structure similar to γ-CrOOH, where the bonding between chained Cr-octahedra is through monodentate mononuclear corner sharing with an interatomic distance of ~3.9 Å (Fendorf et al., 1994). By contrast, our fitting results, with a Cr-Cr interatomic distance at 3.43-3.51 Å (path 4 in Table 1, Fig. 2B&C), indicate a bidentate binuclear corner sharing structure. Such bidentate binuclear corner sharing is similar to the structure of guyanaite (β-CrOOH, structural models provided in Fig. S2); however, the interatomic distance of Cr-Cr (path 4, Table 1, Fig. 2B&C) is 0.1 Å shorter than the corresponding path of long range ordered guyanaite (3.6 Å) (Jahn et al., 2012). Such a shortened distance can be tentatively attributed to the accommodation of Cr onto clay surfaces, which induces necessary connection adjustments between Cr chains (the Nano effect). Additionally, the observation of a Cr-Si bond (path 3 in Table 1, Fig. 2B&C), at an interatomic distance of 3.56-3.60 Å (with a coordination number around 4 for illite and montmorillonite, and 2 for kaolinite), indicates the manner of Cr(III) precipitation on clay minerals is through the substitution of some octahedrally coordinated Al by some octahedrally coordinated Cr, although the interatomic distance of Cr-Si is slightly larger than that of Al-Si in clay minerals (3.22 Å). Previous studies on natural kaolinite and dickite (a monoclinic kaolinite) using electron paramagnetic resonance spectroscopy similarly observed the substitution of Cr(III) for Al(III) when Cr is associated with these clays (Mosser et al., 2018). Our results confirm that the substitution of Cr(III)-bearing octahedra into the Al(III)-octahedral sheet connects clay minerals and Cr(III)-hydroxide, which is common across all three types of clay minerals considered here.

Another means to assess the bonding environment is through determination of the Debye-Waller (DW) factor. This is a parameter that assesses the stability of the local trace element structure, with a lower DW factor indicating a more stable structure. We calculate the DW factors for Cr-Cr, Cr-Al, and Cr-Si (paths 2, 3, and 4 in Table 1, respectively), and find that for illite and montmorillonite at pH 6 the DW factors are higher than that at pH 8. For instance, the DW factors of Cr-Al and Cr-Cr (paths 2-1 and 2-2 in Table 1) for montmorillonite at pH 6 are 0.0040 and 0.0050, respectively, compared to 0.0021 and 0.0021 at pH 8. In particular, the DW factor for Cr-Si (path 3) of illite at pH 6 reaches the upper limit of its acceptable range (0.01). This phenomenon indicates that the stability of these bonds is stronger at pH 8 compared to pH 6. As such, we conclude that the Cr(III) precipitates (indicated by Cr-Cr in paths 2, 4) and surface substitution onto clay surfaces (indicated by Cr-Al and Cr-Si in paths 2, 3) are more stable at pH 8 than at pH 6.

3.2. Cr(III) surface precipitation model

Our fitting results indicate that the replacement of some octahedrally coordinated Al(III) by some octahedrally coordinated Cr(III) in the octahedral layer of all three studied clays occurred during Cr(III) incorporation (Table 1, paths 2-1 and 3, Fig. 2B&C). To illustrate the local structure of Cr(III) substitution onto clay surfaces, two proposed surface replacement models were tested to back-fit the experimental spectra; (1) a single Cr-octahedron substitution, and (2) a paired Cr-octahedra substitution (structural models provided in Fig. S3). FDMNES XANES modeling was performed upon these two Cr local structural models and the calculated results were compared to experimental results (Fig. S4). The results of the paired Cr-octahedra substitution model show a better

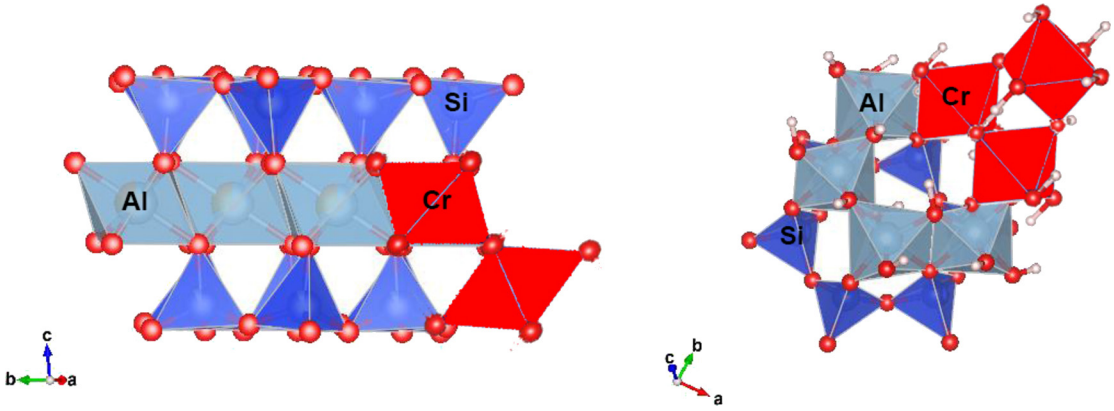

Fig. 3. A model of Cr incorporation into the Al-octahedral sheet of clay minerals. Left figure: side view of clay structure showing the substitution of an Al-octahedron by a Cr-octahedron. Right figure: 3D view of the same clay structure.

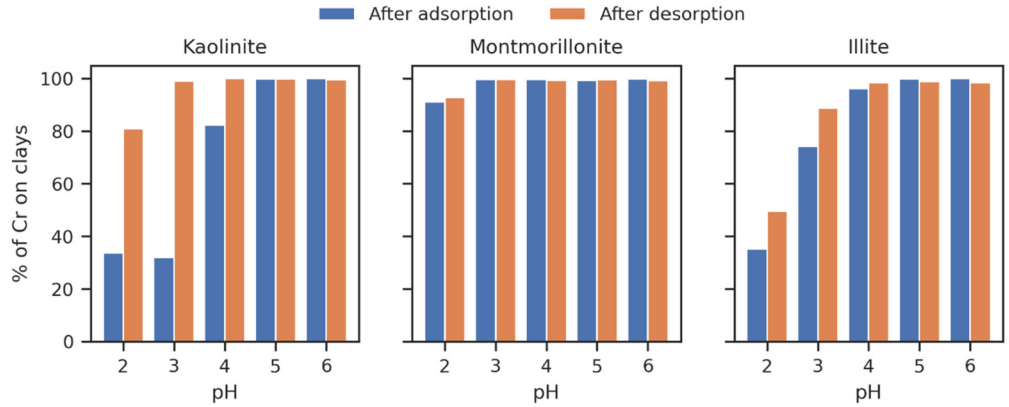

Fig. 4. A comparison between Cr(III) adsorption from solution onto three different clay minerals (blue bar) and the desorption of Cr(III) from previously Cr(III)-spiked clays (orange bar) under different pH conditions.

match for peak positions than the single Cr-octahedron substitution model for kaolinite (Fig. S4A). Most conspicuously, calculated results for the single Cr-octahedron substitution model for montmorillonite show a strong pre-edge "a" feature which differs from the experimental data.

Based on these results, we propose that during Cr(III) precipitation, atomic rearrangement occurs, and paired edge-sharing Cr(III) octahedra replace two Al(III)-octahedra on the clay surfaces. These Cr(III)-replaced octahedra then serve as an interface between the clay minerals and the precipitated Cr(III)-hydroxide, guyanaite. The bonding between the replaced paired-Cr(III)-octahedra and precipitated Cr(III)-hydroxide is through a bidentate binuclear corner sharing complex (Fig. 3).

3.3. Implications for soil profiles and Cr mobilization to the oceans

The removal of one Si-tetrahedral sheet from illite/montmorillonite as it transforms to kaolinite during intermediate to advanced stages of chemical weathering results in a structural change from a three-layer to a two-layer type of clay. This process exposes more Al(III)-octahedra for Cr(III)-octahedral surface precipitation and substitution, which then facilitates higher Cr(III) retention capacities in kaolinite-rich weathering substrates compared to those where montmorillonite or illite is more abundant.

Our Cr(III) desorption experiments showed that kaolinite, which had previously been spiked with Cr(III), retained over 80% of the Cr(III) on its surfaces even after being leached in highly acidic conditions (pH 2). Interestingly, non-spiked kaolinite adsorbed ~35% of the Cr(III) in solution at pH 2. This irreversibility of Cr(III) adsorption and desorption (as indicated by the difference between adsorption and desorption in Fig. 4) is particularly obvious for kaolinite, and points to the highly stable nature of Cr(III) precipitates on the surface of kaolinite (Fig. 4). This, in turn, has broad implications for Cr accumulation in different weathering substrates and the subsequent erosion of such substrates to produce the fine-grained clastic sediment that is cycled to marine environments.

In modern weathering profiles with variable extents of alteration, the residual enrichment of Cr in resistant minerals (e.g., spinel) and/or a close association of Cr(III) with Fe(III) oxyhydroxides (e.g., ferrihydrite, goethite, hematite), with or without preceding Cr(VI) formation by Mn-oxides and back-reduction by Fe(II), is well documented (Zhang et al., 2021; Wille et al., 2018). However, some ultramafic parent rocks have a significant budget of Cr in silicate minerals with a high susceptibility to chemical weathering (olivine and pyroxene) that can readily liberate Cr (e.g., Oze et al., 2004), and advanced weathering conditions can develop discrete horizons or regions selectively enriched in Al due to the greater redox-, acid-, or organic ligand-driven mobility of Fe(II)/Fe(III) relative to Al(III) (Widdowson, 2007). As such, the development of kaolinite and its precursor clay minerals can sequester some or all of early released Cr(III) (Fendorf, 1995), making this Cr(III) less amenable to (1) subsequent liberation as aqueous or colloidal Cr(III) under acidic and/or low-Eh conditions or ligand-rich systems (e.g., conditions described by Saad et al., 2017; Babechuk et al., 2018; and in the overview in Pan and Giammar, 2020); and (2) oxidation of Cr(III) to Cr(VI) by Mn-oxides under higher Eh conditions (e.g., Bishop et al., 2014). Indeed, some studies have shown that the adsorption/coprecipitation of Cr(III) on/with Fe(III) (oxyhydr)oxides alone cannot explain the Cr concentration variations in some laterite profiles (e.g., granite-hosted profile stud-

ied by Berger and Frei, 2014). Thus, while Cr cycling as Cr(III) or Cr(VI) during chemical weathering is a complex function of parent rock mineralogy, Eh-pH, and secondary development of mineral phases, it is argued that clay minerals such as smectites, kaolinite, halloysite, and possibly more advanced post-kaolinite products like gibbsite or boehmite, exert a fundamental and underappreciated control on the immobilization and fate of Cr. We argue that this becomes particularly pertinent when the specific conditions of parent rock type (Cr in weathering susceptible minerals), low pH (promoting Cr(III) mobility), advanced weathering (promoting formation of kaolinite over other clays), and low Eh (poor Fe(III) and Mn(III)/(IV) oxyhydroxide development) converge.

When considering the ancient Earth, we hypothesize that the aforementioned convergence could have been most readily reached at the Earth's surface in the Paleoproterozoic, specifically at the onset of the GOE. Low but sustained levels of atmospheric O_2 – leading to oxidation of pyrite and siderite – could have locally developed acid weathering conditions that promoted Cr(III) solubility but not Fe(III) oxyhydroxide particle formation (Konhauser et al., 2011; Bachan and Kump, 2015), and thus greater association of Cr(III) with clay minerals without widespread Cr(III) oxidation to Cr(VI). The erosion of clay minerals that accumulated and incorporated Cr(III), from the position of formation in a weathering profile up to the point of aqueous pH conditions being unfavorable for the aqueous transport of Cr(III), provides an alternative explanation for the high abundance of Cr above crustal background in IF deposited between 2.45 and 2.32 Ga than the purely soluble Cr(III) model originally proposed by Konhauser et al. (2011). This is an attractive idea as it would reconcile the outstanding problem with the acidic stream/groundwater hypothesis where rock buffering would necessarily have had to be insufficient to neutralize acidic riverine flow before reaching the oceans. In other words, a purely soluble Cr(III) transport model would require the sites of weathering to be in close proximity to the coast. By contrast, if Cr(III) was adsorbed to clay particles, during chemical weathering or along a pathway of fluvial transport, the sites of weathering could have been anywhere upstream. This is indirectly supported by recent experimental evidence for the potential of kaolinite to act as a "phosphate shuttle" between terrestrial and marine environments, which may have been one of the main mechanisms by which P was supplied to seawater following the GOE (Hao et al., 2021). Such terrestrial conditions with low-pH driven Cr(III) solubility converging with kaolinite particle interaction would not have been widespread during the preceding Archean when pyrite (and at times siderite) were more stable at the surface, or after ca. 2.3 Ga when widespread terrestrial Fe(III)-oxyhydroxides formed in weathering profiles and during fluvial sediment diagenesis (i.e., as preserved in paleosols and red beds, respectively). The latter of these time periods marks the appearance of conditions where widespread acid-driven weathering cannot be inferred, and stable Fe(III)-oxyhydroxides particles would have played a greater competing role with clay minerals in near-source Cr(III) scavenging.

To further test whether clays were important for post-GOE Cr(III) transport, we updated the Cr database originally presented in Konhauser et al. (2011) by adding 153 additional literature analyses and bringing the total number of samples with Cr, Al, and Ti data to 838, in order to interrogate the relationship between Cr and clay particles (Fig. 5). The previous study of Konhauser et al. (2011) focused on Cr/Ti ratios as proxy for authigenic enrichment of Cr in IF (see Fig. 1A&B and Section 1), whereas this study instead uses Cr/Al ratios (Fig. 5A&B) to form a more direct relationship to Al-rich clay minerals. Briefly, the Cr/Al ratios in IF through time (Fig. 5A) and the Cr/Al ratios as a function of Al_2O_3 (Fig. 5B) reveal the same overall story as Cr/Ti (Fig. 1A&B), which is discussed here with division into 4 age bins (>2.5 Ga, 2.5-2.3 Ga, 2.3-0.8 Ga, and <0.8 Ga). Broadly, median IF Cr/Al ratios in all ages of IF are comparable to the spread of Cr/Al ratios in average igneous rocks from the Archean to Proterozoic, as well as the restored "juvenile" upper crustal composition across this age range (Condie, 1993) (Fig. 5C&E). Ratios of Cr/Al exceeding crustal values are evident in IF of all ages; however, the most prominent enrichments in Cr are evident in IF deposited between 2.5 and 2.3 Ga, and after 0.8 Ga (Fig. 5C). The Cr/Al in IF record is further interrogated by examining Cr/Al in each age bin divided into high-detritus (>1 wt.% Al_2O_3; including Fe-rich mudrocks and IF intercalated with volcaniclastic material) and low-detritus (<1 wt.% Al_2O_3) IF samples. In general, high detritus IF exhibit lower Cr/Al ratios compared to low detritus IF. Nevertheless, both high and low detritus IF deposited between 2.5 and 2.3 Ga show a notable shift towards higher Cr/Al ratios compared to other age bins.

Variation in the Cr/Al ratios of Archean IF (>2.5 Ga) compared to average crustal rocks can be attributed to local catchment geology (higher Cr/Al where mafic-ultramafic rocks are present, lower Cr/Al where evolved rocks such as TTGs and granite dominate) and/or sedimentary particle contamination with non-clay Cr-rich minerals (e.g., chromite spinels) that were more abundant at the surface from mafic-ultramafic rock sources at the time. However, that the median Cr/Al ratios in Archean IF overlap with crustal averages is consistent with limited Cr solubility during chemical weathering and thus transport of particles with Cr/Al ratios similar to source rocks. The slightly higher Cr/Al ratios in low detritus samples of this age can be explained by minor contamination with non-clay Cr-rich minerals or minor authigenic enrichment from soluble Cr(III) sourced from hydrothermal fluids (e.g., Sander and Koshinsky, 2000), especially in exhalative IF.

Between 2.5 and 2.3 Ga, the shift to higher Cr/Al ratios in high detritus samples than in both the preceding Archean and the remaining period of the Proterozoic is best reconcilable through the transport of Cr into shallow marine systems via clay particles that had scavenged and incorporated additional Cr in the terrestrial sedimentary realm – the central proposal of this study. The highest of these Cr/Al ratios are similar to Cr/Al ratios measured in natural Cr-rich clay minerals (Cr-montmorillonite, Cr-nontronite, Cr-halloysite) (Mitsis et al., 2018, and reference therein) (Fig. 5D). The latter Cr-bearing clays are typically formed in the hydrothermal alteration of ultramafic rock, but nonetheless attest to the high Cr/Al achievable in clay minerals during fluid-rock interaction. Arguably, higher Cr/Al in high-detritus IF could also be explained by the erosion of a higher abundance of mafic-ultramafic rock (e.g., variably altered peridotite) exposed at the time, but this scenario is not reconcilable with the decreasing abundance of such rock types from the Archean into the Proterozoic based on other proxy records (e.g., Konhauser et al., 2009; Kamber, 2010). In other words, while a high-Cr rock source is a requirement for initial sources of Cr(III), the declining abundance of such rock types at the surface would amplify the need for aqueous Cr(III)-clay mineral interaction in the terrestrial environment. The origin of higher Cr/Al in low-detritus IF samples deposited between 2.5 and 2.3 Ga is inherently more ambiguous and could include, beyond local detritus with different mineralogy and perhaps local redistribution of Cr during metamorphism, free soluble Cr(III) sourced from low-pH weathering in coastal environments (as per the model of Konhauser et al., 2011), Cr(III) associated with Fe-oxides, and, perhaps minor amounts of soluble Cr(VI) generated in terrestrial environments and reduced in marine waters (Frei et al., 2009).

The return to lower Cr/Al in IF deposited between 2.3 and 0.8 Ga, similar to values for Archean IF, is strong evidence for low-pH weathering no longer being a major driver of Cr(III) mobility in weathering profiles and return to eroded detritus having Cr/Al that closely reflects average crustal rock sources. For IF (and ironstones) deposited <0.8 Ga, the high detritus IF having near-crustal Cr/Al ratios reflects the limited overall solubility of Cr species, similar

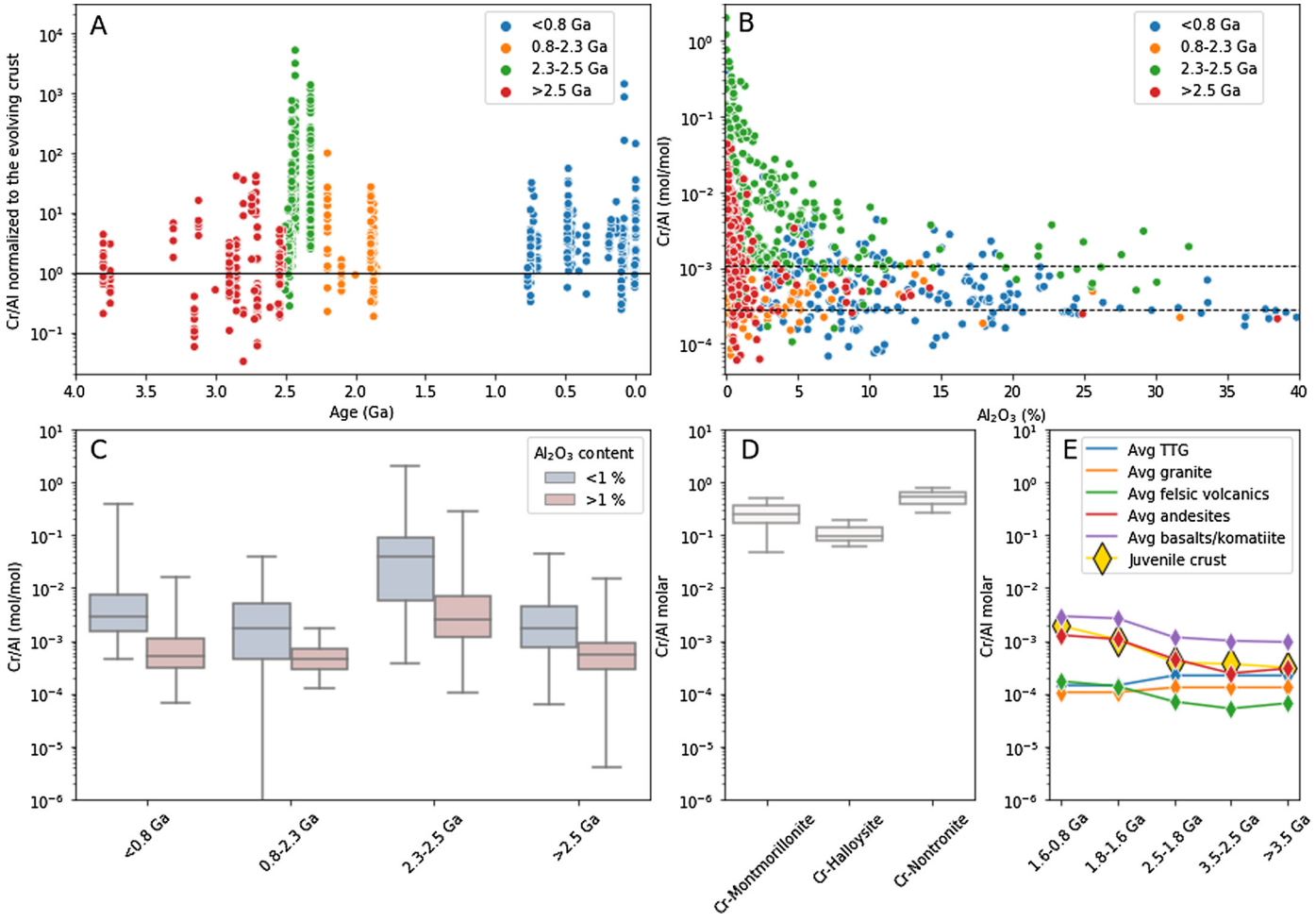

Fig. 5. The database for Cr/Al ratios in IF and its comparison with Cr/Al ratios in igneous rocks and Cr-rich clays. (A) Normalized Cr/Al ratios in IF as a function of geological time; (B) Cross-plot of Al_2O_3 abundance versus molar Cr/Al ratios in IF samples; (C) A box and whisker plot of Cr/Al ratios in IF samples over different time bins; (D) A box and whisker plot of Cr/Al ratios in Cr-rich clays (data in Mitsis et al., 2018, and reference therein); (E) Cr/Al ratios in igneous rocks and juvenile crust (data in Condie, 1993). The upper and lower dashed lines in panel B correspond to the molar Cr/Al ratios expected for upper continental crust from 3.5 to 2.5 Ga and <0.2 Ga, respectively, based on the restoration model of Condie (1993). "TTG" in panel G represents tonalite-trondhjemite-granodiorite, and "juvenile crust" stands for the restoration model for the juvenile crust in Condie (1993). Updated from Konhauser et al. (2011).

to other periods in Earth history outside of 2.5-2.3 Ga. However, the shift to significantly higher Cr/Al ratios in low detritus IF likely reflects the growth of the additional soluble Cr pathway into the oceans that is comparable to present day – Cr(VI) generated by oxidative weathering on land.

Key to the aforementioned interpretations are the absence of significant stable Cr isotope variations in the IF units making up the compilation (Frei et al., 2009), as discussed in Konhauser et al. (2011), such that soluble Cr(VI) formation during weathering and delivery to oceans cannot be easily inferred from the IF Cr isotope record prior to the Neoproterozoic. This scenario is compatible with the limited extent of terrestrial Cr(III) oxidation to Cr(VI) inferred from the paleosol Cr isotope record overlapping this period (Babechuk et al., 2017, 2019; Toma et al., 2019; Colwyn et al., 2019). Some studies have even argued that local Cr(III) mobility in weathering profiles may have been more common than previously assumed at times across the wider Paleoproterozoic (e.g., at ca. 1.9-1.8 Ga) when Cr was hosted in especially weathering-susceptible Cr-bearing silicates, such as epidote, prior to subaerial weathering (Sindol et al., 2020) (i.e., compared to when Cr was either locked in weathering-resistant oxides or mobilized only after oxidation to Cr(VI)); a more complete analysis of ancient Cr weathering behavior in paleosols is needed. It is also noteworthy that organic ligands can potentially mobilize Al (Beaty and Planavsky, 2021), which could further increase Cr/Al ratios in clays in the surface weathering environment. Overall, data appear to converge from both terrestrial and marine Cr records in implicating a greater role of clay minerals as a carrier of Cr(III) from land to the oceans during the periods of the GOE when a low-pH weathering and aquatic environment was supported.

4. Summary

Our experimental study offers new insights into the impact of clay minerals (kaolinite, montmorillonite, illite) on the geochemical cycling of Cr(III) – specifically, the mechanisms whereby Cr(III) can substitute into the clay mineral structure, most prominently kaolinite, such that it becomes tightly bound and stable while weathering and subsequent mass transport removes other elements. During intermediate-to-advanced chemical weathering, not only does the production of high levels of acidity promote the solubilization of Cr(III) from primary Cr-bearing minerals, but parent rock minerals are more readily weathered to kaolinite – ideal for the adsorption of Cr(III). These conditions are expected locally in some modern advanced Al-rich weathering substrates (e.g., bauxites), but are also hypothesized to have been particularly important during periods in Earth's history when acid weathering could have been more widespread and converged with atmospheric O_2 levels that were still too low to readily form terrestrial Fe(III)-oxyhydroxides.

Such a perfect storm of environmental conditions may have been restricted to the immediate aftermath of the GOE, between ca. 2.45 and 2.32 Ga, and could help explain high abundances of Cr preserved in IF deposited at this time, if Cr(III) was shuttled to the oceans bound to kaolinite. Throughout the wider sedimentary record prior to this, Cr(III) was also liable to be transported to the oceans bound to clays, but without extensive Cr(III) solubility in terrestrial environments prior to Cr(III), the detritus retained near-crustal Cr/Al ratios.

CRediT authorship contribution statement

K.O.K., D.S.A., K.M., K.K., Y.T., P.S., M.G.B., N.J.P. and W.H. conceived the study; W.H. performed the Cr adsorption/precipitation experiments, pH edges experiments, and collected EXAFS spectra; N.C. and W.S. helped with EXAFS analysis and structural model development. L.J.R. compiled and updated the database for Cr abundance in iron formations; W.H. and K.O.K. wrote the manuscript with input from all co-authors.

Declaration of competing interest

The authors declare that they have no known competing financial interests or personal relationships that could have appeared to influence the work reported in this paper.

Acknowledgements

This work was supported by NSERC Discovery Grants to K.O.K. (RGPIN-165831), D.S.A. (RGPIN-2020-05289), L.J.R. (RGPIN-2021-02523) and M.G.B. (RGPIN-2017-05028). Synchrotron work was conducted with approval from Canadian Light Source (Proposal No. 9476). We thank Scott Fendorf for providing valuable comments during the writing of this manuscript.

Appendix A. Supplementary material

Supplementary material related to this article can be found online at https://doi.org/10.1016/j.epsl.2022.117503.

References

Albut, G., et al., 2018. Modern rather than Mesoarchaean oxidative weathering responsible for the heavy stable Cr isotopic signatures of the 2.95 Ga old Ijzermijn iron formation (South Africa). Geochim. Cosmochim. Acta 228, 157–189. https://doi.org/10.1016/j.gca.2018.02.034.

Babechuk, M.G., Kleinhanns, I.C., Reitter, E., Schoenberg, R., 2018. Kinetic stable Cr isotopic fractionation between aqueous Cr(III)-Cl-H_2O complexes at 25 °C: implications for Cr(III) mobility and isotopic variations in modern and ancient natural systems. Geochim. Cosmochim. Acta 222, 383–405. https://doi.org/10.1016/j.gca.2017.10.002.

Babechuk, M.G., Kleinhanns, I.C., Schoenberg, R., 2017. Chromium geochemistry of the ca. 1.85 Ga Flin Flon paleosol. Geobiology 15, 30–50. https://doi.org/10.1111/gbi.12203.

Babechuk, M.G., Weimar, N.E., Kleinhanns, I.C., Eroglu, S., Swanner, E.D., Kenny, G.G., Kamber, B.S., Schoenberg, R., 2019. Pervasively anoxic surface conditions at the onset of the Great Oxidation Event: new multi-proxy constraints from the Cooper Lake paleosol. Precambrian Res. 323, 126–163. https://doi.org/10.1016/j.precamres.2018.12.029.

Bachan, A., Kump, L.R., 2015. The rise of oxygen and siderite oxidation during the Lomagundi Event. Proc. Natl. Acad. Sci. USA 112, 6562–6567. https://doi.org/10.1073/pnas.1422319112.

Beaty, B.J., Planavsky, N.J., 2021. A 3 b.y. record of a biotic influence on terrestrial weathering. Geology 49, 407–411. https://doi.org/10.1130/G47986.1.

Berger, A., Frei, R., 2014. The fate of chromium during tropical weathering: a laterite profile from Central Madagascar. Geoderma 213, 521–532. https://doi.org/10.1016/j.geoderma.2013.09.004.

Bishop, M.E., Glasser, P., Dong, H., Arey, B., Kovarik, L., 2014. Reduction and immobilization of hexavalent chromium by microbially reduced Fe-bearing clay minerals. Geochim. Cosmochim. Acta 133, 186–203. https://doi.org/10.1016/j.gca.2014.02.040.

Boski, T., Herbosch, A., 1990. Trace elements and their relation to the mineral phases in the lateritic bauxites from southeast Guinea Bissau. Chem. Geol. 82, 279–297. https://doi.org/10.1016/0009-2541(90)90086-M.

Canfield, D.E., Zhang, S., Frank, A.B., Wang, X., Wang, H., Su, J., Ye, Y., Frei, R., 2018. Highly fractionated chromium isotopes in Mesoproterozoic-aged shales and atmospheric oxygen. Nat. Commun. 9, 1–11. https://doi.org/10.1038/s41467-018-05263-9.

Colwyn, D.A., Sheldon, N.D., Maynard, J.B., Gaines, R., Hofmann, A., Wang, X., Gueguen, B., Asael, D., Reinhard, C.T., Planavsky, N.J., 2019. A paleosol record of the evolution of Cr redox cycling and evidence for an increase in atmospheric oxygen during the Neoproterozoic. Geobiology 17, 579–593. https://doi.org/10.1111/gbi.12360.

Condie, K.C., 1993. Chemical composition and evolution of the upper continental crust: contrasting results from surface samples and shales. Chem. Geol. 104, 1–37. https://doi.org/10.1016/0009-2541(93)90140-E.

Crowe, S.A., et al., 2013. Atmospheric oxygenation three billion years ago. Nature 501, 535–538. https://doi.org/10.1038/nature12426.

Eary, L.E., Rai, D., 1987. Kinetics of chromium (III) oxidation to chromium (VI) by reaction with manganese dioxide. Environ. Sci. Technol. 21, 1187–1193. https://doi.org/10.1021/es00165a005.

Farquhar, J., et al., 2011. Geological constraints on the origin of oxygenic photosynthesis. Photosynth. Res. 107, 11–36. https://doi.org/10.1007/s11120-010-9594-0.

Fendorf, S.E., 1995. Surface reactions of chromium in soils and waters. Geoderma 1–2, 55–71. https://doi.org/10.1016/0016-7061(94)00062-F.

Fendorf, S.E., Lamble, G.M., Stapleton, M.G., Kelley, M.J., Sparks, D.L., 1994. Mechanisms of chromium (III) sorption on silica. 1. Chromium (III) surface structure derived by extended x-ray absorption fine structure spectroscopy. Environ. Sci. Technol. 28, 284–289. https://doi.org/10.1021/es00051a015.

Fendorf, S.E., Zasoski, R.J., 1992. Chromium (III) oxidation by .delta.-manganese oxide (MnO2). 1. Characterization. Environ. Sci. Technol. 26, 79–85. https://doi.org/10.1021/es00025a006.

Frei, R., Gaucher, C., Poulton, S.W., Canfield, D.E., 2009. Fluctuations in Precambrian atmospheric oxygenation recorded by chromium isotopes. Nature 461, 250–253. https://doi.org/10.1038/nature08266.

Gilleaudeau, G.J., et al., 2016. Oxygenation of the mid-Proterozoic atmosphere: clues from chromium isotopes in carbonates. Geochem. Perspect. Lett. 2, 178–187. https://doi.org/10.7185/geochemlet.1618.

Griffin, R.A., Au, A.K., Frost, R.R., 1977. Effect of pH on adsorption of chromium from landfill-leachate by clay minerals. J. Environ. Sci. Health, Part A 12, 431–449. https://doi.org/10.1080/10934527709374769.

Hao, W., et al., 2019. The impact of ionic strength on the proton reactivity of clay minerals. Chem. Geol. 119294. https://doi.org/10.1016/j.chemgeo.2019.119294.

Hao, W., et al., 2021. The kaolinite shuttle links the Great Oxidation and Lomagundi events. Nat. Commun. 12, 1–7. https://doi.org/10.1038/s41467-021-23304-8.

Ichikawa, M., Gustafsson, T., Olovsson, I., Tsuchida, T., 1999. Powder neutron-diffraction profile analysis of zero-dimensional H-bonded crystal HCrO2. J. Phys. Chem. Solids 60, 1875–1880. https://doi.org/10.1016/S0022-3697(99)00189-4.

Jahn, S., et al., 2012. Pressure-induced hydrogen bond symmetrisation in guyanaite, β-CrOOH: evidence from spectroscopy and ab initio simulations. Eur. J. Mineral. 24, 839–850. https://doi.org/10.1127/0935-1221/2012/0024-2228.

Kadir, S., Aydoğan, M.S., Elitok, Ö., Helvaci, C., 2015. Composition and genesis of the nickel-chrome-bearing nontronite and montmorillonite in lateritized ultramafic rocks in the Muratdağı region (Uşak, western Anatolia), Turkey. Clays Clay Miner. 63, 163–184. https://doi.org/10.1346/CCMN.2015.0630302.

Kamber, B., 2010. Archean mafic-ultramafic volcanic landmasses and their effect on ocean-atmosphere chemistry. Chem. Geol. 274, 19–28. https://doi.org/10.1016/j.chemgeo.2010.03.009.

Konhauser, K.O., Pecoits, E., Lalonde, S.V., Papineau, D., Nisbet, E.G., Barley, M.E., Arndt, N.T., Zahnle, K., Kamber, B.S., 2009. Oceanic nickel depletion and a methanogen famine before the Great Oxidation Event. Nature 458, 750–753. https://doi.org/10.1038/nature07858.

Konhauser, K.O., et al., 2011. Aerobic bacterial pyrite oxidation and acid rock drainage during the Great Oxidation Event. Nature 478, 369–373. https://doi.org/10.1038/nature10511.

McClain, C.N., Maher, K., 2016. Chromium fluxes and speciation in ultramafic catchments and global rivers. Chem. Geol. 426, 135–157. https://doi.org/10.1016/j.chemgeo.2016.01.021.

Mitsis, I., et al., 2018. Chromium-bearing clays in altered ophiolitic rocks from Crommyonia (Soussaki) volcanic area, Attica, Greece. Appl. Clay Sci. 162, 362–374. https://doi.org/10.1016/j.clay.2018.06.016.

Mosser, C., Petit, S., Mestdagh, M., 2018. ESR and IR evidence for chromium in kaolinites. Clay Miner. 28, 353–364. https://doi.org/10.1180/claymin.1993.028.3.02.

Oze, C., Bird, D.K., Fendorf, S., 2007. Genesis of hexavalent chromium from natural sources in soil and groundwater. Proc. Natl. Acad. Sci. USA 104, 6544–6549. https://doi.org/10.1073/pnas.0701085104.

Oze, C., Fendorf, S., Bird, D.K., Coleman, R.G., 2004. Chromium geochemistry of serpentine soils. Int. Geol. Rev. 46, 97–126. https://doi.org/10.2747/0020-6814.46.2.97.

Pan, C., Giammar, D., 2020. Interplay of transport processes and interfacial chemistry affecting chromium reduction and reoxidation with iron and manganese. Front. Environ. Sci. Eng. 14, 81. https://doi.org/10.1007/s11783-020-1260-y.

Planavsky, N.J., et al., 2014. Low Mid-Proterozoic atmospheric oxygen levels and the delayed rise of animals. Science 346, 635–638. https://doi.org/10.1126/science.1258410.

Rai, D., Eary, L., Zachara, J.M., 1989. Environmental chemistry of chromium. Sci. Total Environ. 86, 15–23. https://doi.org/10.1016/0048-9697(89)90189-7.

Reinhard, C.T., Planavsky, N.J., Robbins, L.J., Partin, C., Gill, B.C., Lalonde, S.V., Bekker, A., Konhauser, K.O., Lyons, T.W., 2013. Proterozoic ocean redox and biogeochemical stasis. Proc. Natl. Acad. Sci. USA 110, 5357–5362. https://doi.org/10.1073/pnas.1208622110.

Rye, R., Holland, H.D., 1998. Paleosols and the evolution of atmospheric oxygen: a critical review. Am. J. Sci. 298, 621–672. https://doi.org/10.2475/ajs.298.8.621.

Saad, E.M., Wang, X., Planavsky, N.J., Reinhard, C.T., Tang, Y., 2017. Redox-independent chromium isotope fractionation induced by ligand-promoted dissolution. Nat. Commun. 8, 1590. https://doi.org/10.1038/s41467-017-01694-y.

Sajidu, S., Persson, I., Masamba, W., Henry, E., 2008. Mechanisms of heavy metal sorption on alkaline clays from Tundulu in Malawi as determined by EXAFS. J. Hazard. Mater. 158, 401–409. https://doi.org/10.1016/j.jhazmat.2008.01.087.

Sander, S., Koshinsky, A., 2000. Onboard-ship redox speciation of chromium in diffuse hydrothermal fluids from the North Fiji Basin. Mar. Chem. 71, 83–102. https://doi.org/10.1016/S0304-4203(00)00042-6.

Sarı, A., Tuzen, M., Soylak, M., 2007. Adsorption of Pb (II) and Cr (III) from aqueous solution on Celtek clay. J. Hazard. Mater. 144, 41–46. https://doi.org/10.1016/j.jhazmat.2006.09.080.

Sindol, G.P., Babechuk, M.G., Petrus, J.A., Kamber, B.S., 2020. New insights into Paleoproterozoic surficial conditions revealed by 1.85 Ga corestone-rich saprolith. Chem. Geol. 545, 119621. https://doi.org/10.1016/j.chemgeo.2020.119621.

Singer, P.C., Stumm, W., 1970. Acidic mine drainage: the rate-determining step. Science 167, 1121–1123. https://doi.org/10.1126/science.167.3921.1121.

Toma, J., Holmden, C., Shakotko, P., Pan, Y., Ootes, L., 2019. Cr isotopic insights into ca. 1.9 Ga oxidative weathering of the continents using the Beaverlodge Lake paleosol, Northwest Territories, Canada. Geobiology 50, 1223. https://doi.org/10.1111/gbi.12342.

Trolard, F., Bourrie, G., Jeanroy, E., Herbillon, A.J., Martin, H., 1995. Trace metals in natural iron oxides from laterites: a study using selective kinetic extraction. Geochim. Cosmochim. Acta 59, 1285–1297. https://doi.org/10.1016/0016-7037(95)00043-Y.

Widdowson, M., 2007. Laterite and ferricrete. In: Geochemical Sediments and Landscapes, 488 pp.

Wille, M., Babechuk, M.G., Kleinhanns, I.C., Stegmaier, J., Suhr, N., Widdowson, M., Kamber, B.S., Schoenberg, R., 2018. Silicon and chromium stable isotopic systematics during basalt weathering and lateritisation: a comparison of variably weathered basalt profiles in the Deccan Traps, India. Geoderma 314, 190–204. https://doi.org/10.1016/j.geoderma.2017.10.051.

Yang, W., Holland, H.D., 2003. The Hekpoort paleosol profile in Strata 1 at Gaborone, Botswana: soil formation during the Great Oxidation Event. Am. J. Sci. 303, 187–220. https://doi.org/10.2475/ajs.303.3.187.

Zeissink, H., 1969. The mineralogy and geochemistry of a nickeliferous laterite profile (Greenvale, Queensland, Australia). Miner. Depos. 4, 132–152. https://doi.org/10.1007/BF00208049.

Zhang, W., et al., 2021. Rapid sequestration of chelated Cr(III) by ferrihydrite: adsorption and overall transformation of Cr(III) complexes. Colloids Surf. A 11, 12689. https://doi.org/10.1016/j.colsurfa.2021.126819.